Fabrication of Multiresponsive Bioactive Nanocapsules through Orthogonal Self-Assembly**

Yi-Cheun Yeh, Rui Tang, Rubul Mout, Youngdo Jeong, and Vincent M. Rotello

Abstract: *Multifunctional self-assembled systems present platforms for fundamental research and practical applications as they provide tunability of structure, functionality, and stimuli responsiveness. Pragmatic structures for biological applications have multiple design requirements, including control of size, stability, and environmental response. Here we present the fabrication of multifunctional nanoparticle-stabilized capsules (NPSCs) by using a set of orthogonal supramolecular interactions. In these capsules, fluorescent proteins are attached to quantum dots through polyhistidine coordination. These anionic assemblies interact laterally with cationic gold nanoparticles that are anchored to the fatty acid core through guanidinium–carboxylate interactions. The lipophilic core then provides a reservoir for hydrophobic endosome-disrupting agents, thereby generating a system featuring stimuli-responsive release of a payload into the cytosol with fluorescence monitoring.*

Multifunctional nanomaterials are important platforms for "smart" applications, since they combine the properties of their components[1] to provide synergistic systems[2] capable of achieving multiple objectives. Through the appropriate choice of attributes, multifunctional materials can overcome challenges that cannot be solved by their individual components,[3] including the ability to dynamically adjust their properties and functions in response to both endogenous[4] and external[5] environmental stimuli. Several construction challenges, however, must be addressed for these systems to be useful, such as control over the size, stability, and dynamic properties.[6]

Many systems used for bio-nanotechnology employ covalent conjugation approaches to generate stable nanostructures.[7] However, these building elements are fixed, thus making it difficult to further modulate the structure and provide stimuli responsiveness. Supramolecular chemistry provides an alternative fabrication strategy that addresses the construction challenges of multifunctional materials through multiple noncovalent interactions to generate controllable and stimuli-responsive structures.[8] These supramolecular structures are generated through programmed self-assembly of building blocks (e.g. synthetic materials and biomolecules) by using a broad palette of available noncovalent interactions, including hydrogen bonding, hydrophobic interactions, and electrostatic affinities to induce biomimetic assembly.[9] Recent examples of this bio-inspired assembly strategy include hybrid assemblies,[10] peptide amphiphile vesicles,[11] and protocell models.[12]

The integration of nanoparticles (NPs) into supramolecular structures provides access to the physical[13] and structural[14] properties of the particles. In particular, self-assembly of NPs at the liquid–liquid interface provides a straightforward pathway to generate core–shell nanoparticle-stabilized capsules (NPSCs).[15] Seen from a biomedical perspective, the NPSC platform incorporates the unique physicochemical properties of the NPs into the shell while providing an interior hydrophobic space suitable for the transport of drugs and other functional agents.[16]

Here we present the integration of multiple functional building blocks into an NPSC-based platform by means of diverse supramolecular interactions (Figure 1). In these constructs, CdSe/ZnS core–shell quantum dots (QDs) are conjugated with polyhistidine-tagged proteins by exploiting the metal affinity of the histidine residues on the QD surface. These anionic QD–protein complexes further interact electrostatically with cationic gold nanoparticles (AuNPs) that are pinned to the capsule surface through a combination of hydrogen bonding and electrostatic interactions with the oil core. The resultant supramolecular nanocapsules demonstrate multifunctional properties in cellular studies, such as fluorescent tracking of intracellular bioconjugates, stimuli-responsive protein release, and co-delivery of proteins and hydrophobic endosome-disrupting agents to provide cytosolic protein delivery.
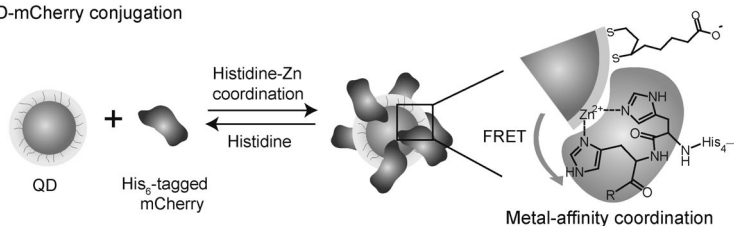
Dihydrolipoic acid functionalized CdSe/ZnS core–shell QDs (QDs_DHLA) generate stable assemblies with polyhistidine-tagged proteins through metal-affinity coordination.[17] For our studies, hexahistidine-tagged red fluorescent protein mCherry ($\lambda_{em} = 610$ nm) was conjugated to green-emitting QD_DHLA ($\lambda_{em} = 550$ nm; Figure 1a). The emission spectrum of the QD overlapped with the absorption spectrum of mCherry (see Figure S1a in the Supporting Information), thus enabling the use of fluorescence resonance energy transfer (FRET) to track the association process. The FRET studies of QD–mCherry conjugates were performed in phosphate-buffered saline (PBS, pH 7.4). The loss of the QD emission was accompanied by an increase in the mCherry emission as the number of mCherry molecules per QD (N) increased (see Figure S1b in the Supporting Information). The FRET phenomena of the QD–mCherry conjugates were maintained in PBS containing 10% serum (Figure 2a), thus demonstrat-

[*] Y.-C. Yeh, R. Tang, R. Mout, Y. Jeong, Prof. V. M. Rotello
Department of Chemistry, University of Massachusetts Amherst
710 North Pleasant Street, Amherst, MA 01003 (USA)
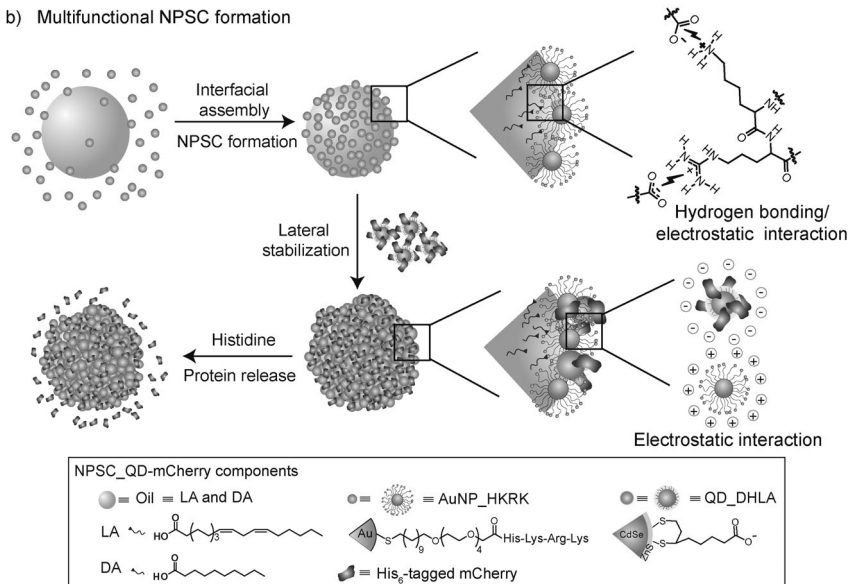E-mail: rotello@chem.umass.edu

Supporting information for this article (Experimental details) is available on the WWW under http://dx.doi.org/10.1002/anie.201400559.

a) QD-mCherry conjugation

Metal-affinity coordination

b) Multifunctional NPSC formation

Hydrogen bonding/electrostatic interaction

Electrostatic interaction

NPSC_QD-mCherry components

Figure 1. a) QD_DHLA and hexahistidine-tagged (His6-tagged) mCherry were conjugated through metal-affinity coordination; this conjugation can be reversed by adding competitive molecules (e.g. histidine). b) Template droplets were generated by agitating AuNP_HKRK (AuNPs functionalized with peptide (histidine-lysine-arginine-lysine)) and oil (linoleic acid (LA) and decanoic acid (DA)) in 5 mM phosphate buffer (pH 7.4), and then the template droplets were transferred into AuNP_HKRK solution followed by lateral noncovalent cross-linking using anionic QD–mCherry conjugates to form NPSC_QD–mCherry.

means of electrostatic interactions to form NPSC_QD–mCherry (Figure 1 b). NPSC_QD-mCherry was characterized by using transmission electron microscopy (TEM; Figure 2c) and dynamic light scattering (DLS; Figure 2d). NPSC_QD–mCherry presented a hydrodynamic diameter of (120 ± 50) nm and a higher stability in serum-supplemented media than the NPSC (Figure 2d and see Figure S3 in the Supporting Information). The formation of stable NPSC_QD–mCherry confirmed the noncovalent cross-linking between anionic QD–mCherry conjugates and cationic AuNPs at the oil–water interface.

The high stability of NPSC_QD–mCherry in serum-supplemented media makes this capsule potentially useful in biological applications. The utility of NPSC_QD–mCherry was tested through uptake studies in HeLa cells, with cellular uptake and distribution analyzed using confocal laser scanning microscopy (CLSM) and flow cytometry. NPSC_QD–mCherry presented a dominant red fluorescence (Figure 3a) inside the cells compared to the control experiments, which included mCherry and QD–mCherry conjugates (see Figure S4a and S4b in the Supporting Information). No green fluorescence was observed in the confocal images, thus indicating the FRET efficiency and stability of the QD–mCherry complexes. Higher intracellular
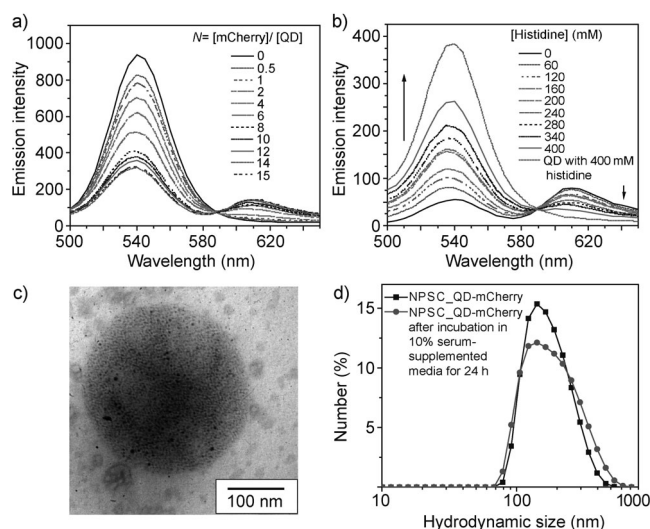
ing the stability of QD–mCherry conjugates in the presence of serum proteins.

An important aspect of conjugation through metal coordination is that the complexes can be disrupted by competing molecules. The release of polyhistidine-tagged protein from the particle surface can be achieved by the treatment of the conjugates with histidine or its analogues (e.g. imidazole).[18] Here we used histidine as a biocompatible external stimulus to investigate the binding events in the QD–mCherry conjugates. After addition of histidine to the solution of QD–mCherry conjugates ($N=6$, where the fluorescence of the QD was quenched by mCherry), the fluorescence recovery of the QDs was accompanied by a decreasing mCherry fluorescence (Figure 2b). The results indicated that histidine can disrupt the FRET process in the QD–mCherry conjugates and release mCherry from the QD surface in a concentration-dependent manner.

We hypothesized that negatively charged QD–mCherry conjugates (zeta potential of the conjugates was ca. −30 mV; see Figure S2 in the Supporting Information) could be used as noncovalent cross-linkers to provide lateral stability to the NPSC structure. Anionic QD–mCherry conjugates and cationic AuNPs were self-assembled at the water–oil interface by

Figure 2. a) Stability of QD–mCherry conjugates in 10% serum-supplemented PBS after 4 h. b) Histidine disrupted the QD–mCherry interactions (QD–mCherry complexes were at a fixed conjugation ratio with $N=6$). c) TEM image of NPSC_QD–mCherry. d) Hydrodynamic diameter of NPSC_QD–mCherry was measured by DLS before and after 24 h incubation in 10% serum-supplemented media.
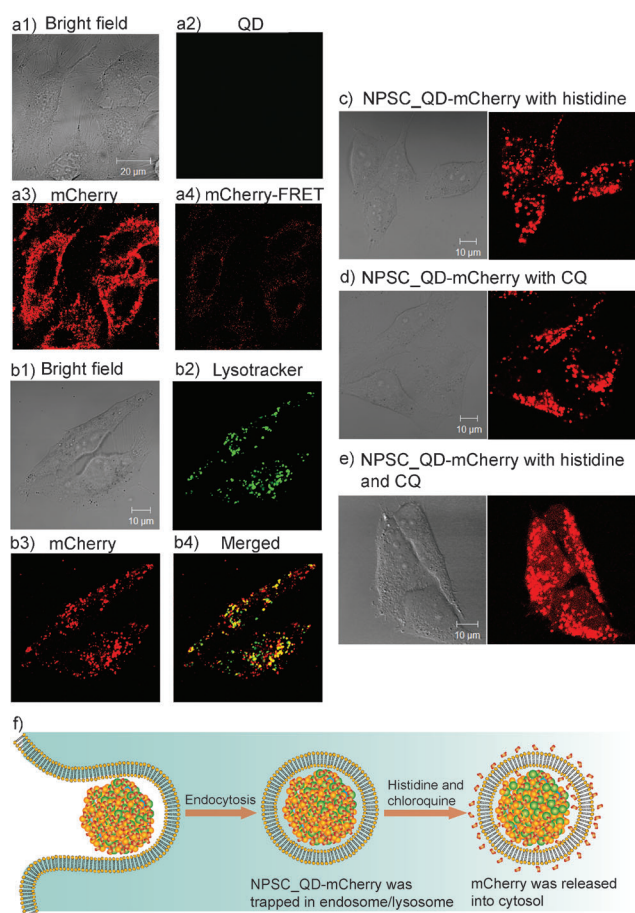
Figure 3. a) NPSC_QD–mCherry ($N=6$) was incubated with HeLa cells for 1 h. a1) Bright-field image, fluorescence images of a2) QD ($\lambda_{ex}=458$ nm, $\lambda_{em}=$ BP 505–530 nm), a3) mCherry ($\lambda_{ex}=543$ nm, $\lambda_{em}=$ LP 650 nm), and a4) FRET signals ($\lambda_{ex}=458$ nm, $\lambda_{em}=$ LP 650 nm). Emission filters: BP = band pass, LP = high pass. b) Co-localization studies of green-emitting lysotracker and NPSC_QD–mCherry ($N=6$). NPSC_QD–mCherry was incubated with HeLa cells for 1 h, and green-emitting lysotracker (100 nm) was incubated with cells for 30 min prior to the microscopy experiments. b1) Bright-field image, and fluorescence images of b2) green-emitting lysotracker and b3) mCherry, and b4) merged fluorescence images. To examine the effect of the external triggers, NPSC_QD–mCherry ($N=6$) was first incubated with HeLa cells for 1 h, and then treated with c) histidine (100 mm), d) CQ (100 μm), and e) co-treated with histidine and CQ for another 1 h. f) Schematic illustration of the endocytosis of NPSC_QD–mCherry and cytosolic release of mCherry upon co-treatment with histidine and CQ.

fluorescence intensity was also observed with NPSC_QD–mCherry relative to controls using flow cytometry (see Figure S4c in the Supporting Information).

The intracellular distribution of NPSC_QD–mCherry was further investigated using green-emitting lysotracker because of the negligible fluorescence of the QDs in the green channel (Figure 3 a2). A significant co-localization of red fluorescent NPSC_QD–mCherry and green fluorescent lysotracker was observed after the incubation with HeLa cells for 1 h (Figure 3 b) and 4 h (see Figure S5 in the Supporting Information), which indicated that NPSC_QD–mCherry was taken up

as expected by endocytosis[19] and subsequently trapped in endosomes/lysosomes.

Endosomal/lysosomal entrapment limits the utility of delivered bio-macromolecules.[20] We investigated the abilities of two orthogonal chemical reagents, histidine and chloroquine (CQ), to serve as stimuli to regulate the intracellular distribution and binding phenomena of QD–mCherry conjugates. Histidine can be used to disassemble the QD–mCherry conjugates as a consequence of the competitive binding toward the hexahistidine tags on mCherry; CQ is a weak base that can destabilize endosomal/lysosomal membranes.[21] NPSC_QD–mCherry was incubated with HeLa cells for 1 h before treatment with each reagent. Punctate fluorescence was observed for mCherry in the cells that had internalized NPSC_QD–mCherry after treatment with histidine or CQ alone (Figure 3 c,d). In contrast, mCherry was distributed throughout the cytosol after co-treatment with histidine and CQ (Figure 3 e). This outcome was verified through two-channel studies, which allows tracking of the QDs and mCherry simultaneously (see Figure S6 in the Supporting Information). These results demonstrated a simple version of an AND logic gate,[22] where both histidine-induced disassembly of QD–mCherry conjugates and CQ-mediated release of the free mCherry from the endosome/lysosome were required for cytosolic access. This release of mCherry was presumably facilitated by the high concentration of intracellular proteins, which would be expected to displace mCherry from the capsules. The uptake mechanism of NPSC_QD–mCherry and cytosolic release of mCherry are summarized in Figure 3 f.

The above experiments demonstrated the combined effects of histidine and CQ as external stimuli in modulating the cytosolic release of mCherry. We next used the hydrophobic core of the NPSC as a reservoir for CQ to form NPSC-CQ_QD–mCherry. After the internalization of NPSC-CQ_QD–mCherry into the cells, punctate fluorescence of mCherry was observed (Figure 4 a, and see Figure S7a in the Supporting Information for a color image), which indicates that, as above, dual triggering was required. As expected, disperse fluorescence of mCherry was observed in the cytosol after delivery of NPSC-CQ_QD–mCherry followed by treatment with histidine (Figure 4 b, and see Figure S7b in the Supporting Information for a color image). Significantly, these studies demonstrated the dual-delivery capability of NPSC-CQ_QD–mCherry; it can deliver both the hydrophilic proteins and hydrophobic endosome-disrupting agents by making use of both its exterior and interior simultaneously.

The results showed qualitatively that the proteins can be released into the cytosol by using appropriate triggers. Fluorescence intensity analysis was used to quantify the cytosolic and vesicular distribution of the intracellular fluorescent proteins.[23] The cytosolic and endosomal/lysosomal fluorescence intensity can be determined by analyzing the fluorescence intensity profiles along the lines in Figure 4 a,b. Pixels with high fluorescence intensities (200–255) in the punctate fluorescent spots were considered to originate from endosomal/lysosomal fluorescence, while pixels with low fluorescence intensities (30–85) observed in the disperse
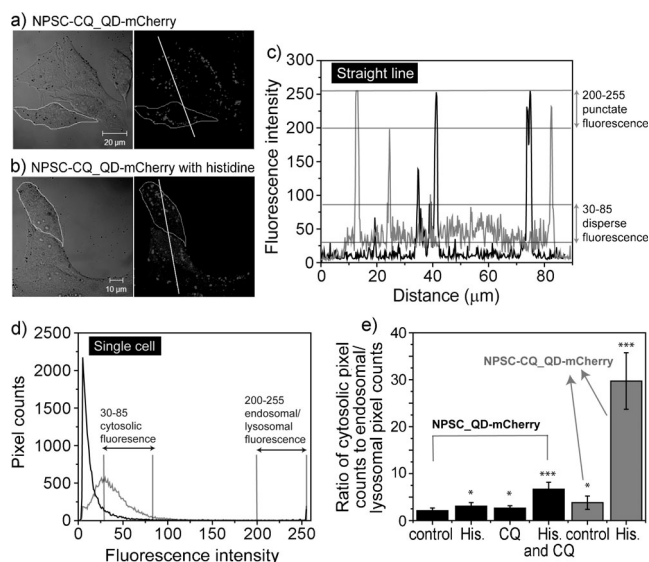
Figure 4. a,b) NPSC-CQ_QD–mCherry (N = 6) was incubated with HeLa cells for 1 h followed by treatment with histidine (100 mM, 1 h). c) Fluorescence intensity profiles along the lines drawn in (a) and (b). Black line: NPSC-CQ_QD–mCherry, gray line: NPSC-CQ_QD–mCherry with histidine. d) Pixel-count histograms of the fluorescence inside the region of interest as marked with white lines in (a) and (b). Black line: NPSC-CQ_QD–mCherry, gray line: NPSC-CQ_QD–mCherry with histidine. e) Ratio of cytosolic pixel counts to endosomal/lysosomal pixel counts of intracellular mCherry under different experimental conditions: NPSC_QD–mCherry only, NPSC_QD–mCherry with histidine, NPSC_QD–mCherry with CQ, NPSC_QD–mCherry with co-treatment of histidine and CQ, NPSC-CQ_QD–mCherry only, and NPSC-CQ_QD–mCherry with histidine (see Figure S7 in the Supporting Information for a color image). His. = histidine. * $p \leq 0.05$, *** $p \leq 0.001$.

fluorescent area were considered to be due to cytosolic fluorescence (Figure 4c).

The fluorescence intensity profile of a single cell was measured to allow analysis of the frequency distribution of pixels with high/low fluorescence intensities. As shown in Figure 4d, cells that had internalized NPSC-CQ_QD–mCherry showed a majority of pixels with very low fluorescence intensities. After treatment with histidine, however, a broad distribution of pixel intensities was observed, in agreement with the reported fluorescence signal distributions of proteins that escape from endocytic vesicles to the cytosol.[23]

The frequency distribution of fluorescence intensities can be used to quantitatively compare the degree of fluorescence distribution in the endosome/lysosome and cytosol.[23a,24] Cytosolic fluorescent pixels (fluorescence intensities 30–85) in the whole cell were counted to determine the percentage of cytosolic mCherry when NPSC_QD–mCherry and NPSC-CQ_QD–mCherry were internalized into cells. Cytosolic fluorescence of mCherry was noticeable with NPSC_QD–mCherry upon co-treatment with histidine and CQ as well as with NPSC-CQ_QD–mCherry on treatment with histidine alone (see Figure S8 in the Supporting Information). The ratio of cytosolic pixel counts (fluorescence intensities 30–85) to endosomal/lysosomal pixel counts (fluorescence intensities 200–255) under different experimental conditions is shown in

Figure 4e. The results indicated that the NPSC-CQ_QD–mCherry internalized into cells treated with histidine presented a significantly higher level of cytosolic fluorescence of mCherry compared to cells that had internalized NPSC_QD–mCherry without any treatment (ca. 10-fold). Moreover, a substantially higher degree of endosomal/lysosomal release was observed with the encapsulated CQ relative to the externally added CQ, presumably as a result of the higher local concentration of CQ in the endosome/lysosome.

In summary, we have fabricated NPSC structures that use multiple supramolecular interactions to provide multifunctional materials. These nanocapsules are stabilized through combinations of supramolecular interactions that impart multifunctionality to the capsules. In particular, these capsules feature a dual-release "AND gate" mechanism, where two stimuli are required for release of the cargo protein to the cytosol. These studies demonstrate that utilization of multiple supramolecular interactions in nanocapsules provides a potent strategy for the creation of responsive systems that serve as potential platforms for next-generation smart materials for biological and functional materials applications.

[1] a) C. E. Ashley, E. C. Carnes, G. K. Phillips, D. Padilla, P. N. Durfee, P. A. Brown, T. N. Hanna, J. W. Liu, B. Phillips, M. B. Carter, N. J. Carroll, X. M. Jiang, D. R. Dunphy, C. L. Willman, D. N. Petsev, D. G. Evans, A. N. Parikh, B. Chackerian, W. Wharton, D. S. Peabody, C. J. Brinker, *Nat. Mater.* **2011**, *10*, 389–397; b) M. Ma, H. R. Chen, Y. Chen, X. Wang, F. Chen, X. Z. Cui, J. L. Shi, *Biomaterials* **2012**, *33*, 989–998; c) S. K. Yen, D. Ja nczewski, J. L. Lakshmi, S. B. Dolmanan, S. Tripathy, V. H. B. Ho, V. Vijayaragavan, A. Hariharan, P. Padmanabhan, K. K. Bhakoo, T. Sudaharan, S. Ahmed, Y. Zhang, S. T. Selvan, *ACS Nano* **2013**, *7*, 6796–6805.
[2] a) J. Park, S. H. Wrzesinski, E. Stern, M. Look, J. Criscione, R. Ragheb, S. M. Jay, S. L. Demento, A. Agawu, P. L. Limon, A. F. Ferrandino, D. Gonzalez, A. Habermann, R. A. Flavell, T. M. Fahmy, *Nat. Mater.* **2012**, *11*, 895–905; b) H. L. Jiang, T. Akita, T. Ishida, M. Haruta, Q. Xu, *J. Am. Chem. Soc.* **2011**, *133*, 1304–1306; c) C. Wang, H. Xu, C. Liang, Y. Liu, Z. Li, G. Yang, L. Cheng, Y. Li, Z. Liu, *ACS Nano* **2013**, *7*, 6782–6795.
[3] a) J. F. Lovell, C. S. Jin, E. Huynh, H. Jin, C. Kim, J. L. Rubinstein, W. C. W. Chan, W. Cao, L. V. Wang, G. Zheng, *Nat. Mater.* **2011**, *10*, 324–332; b) J. B. Song, J. J. Zhou, H. W. Duan, *J. Am. Chem. Soc.* **2012**, *134*, 13458–13469; c) F. Zhang, G. B. Braun, A. Pallaoro, Y. C. Zhang, Y. F. Shi, D. X. Cui, M. Moskovits, D. Y. Zhao, G. D. Stucky, *Nano Lett.* **2012**, *12*, 61–67.
[4] a) T. Chen, M. I. Shukoor, R. W. Wang, Z. L. Zhao, Q. Yuan, S. Bamrungsap, X. L. Xiong, W. H. Tan, *ACS Nano* **2011**, *5*, 7866–7873; b) J. Nam, W. G. La, S. Hwang, Y. S. Ha, N. Park, N. Won, S. Jung, S. H. Bhang, Y. J. Ma, Y. M. Cho, M. Jin, J. Han, J. Y. Shin, E. K. Wang, S. G. Kim, S. H. Cho, J. Yoo, B. S. Kim, S. Kim, *ACS Nano* **2013**, *7*, 3388–3402.
[5] C. Y. Lai, B. G. Trewyn, D. M. Jeftinija, K. Jeftinija, S. Xu, S. Jeftinija, V. S. Y. Lin, *J. Am. Chem. Soc.* **2003**, *125*, 4451–4459.

[6] a) F. Perche, V. P. Torchilin, *J. Drug Delivery* **2013**, 705265–705265; b) K. Salonitis, J. Pandremenos, J. Paralikas, G. Chryssolouris, *Int. J. Adv. Manuf. Technol.* **2010**, *49*, 803–826.

[7] a) T. Liu, X. J. Li, Y. F. Qian, X. L. Hu, S. Y. Liu, *Biomaterials* **2012**, *33*, 2521–2531; b) O. K. Park, J. Y. Hwang, M. Goh, J. H. Lee, B. C. Ku, N. H. You, *Macromolecules* **2013**, *46*, 3505–3511; c) F. Dong, C. S. Ha, *Macromol. Res.* **2012**, *20*, 335–343.

[8] a) S. I. Stupp, V. LeBonheur, K. Walker, L. S. Li, K. E. Huggins, M. Keser, A. Amstutz, *Science* **1997**, *276*, 384–389; b) G. M. Whitesides, B. Grzybowski, *Science* **2002**, *295*, 2418–2421; c) D. Philp, J. F. Stoddart, *Angew. Chem.* **1996**, *108*, 1242–1286; *Angew. Chem. Int. Ed. Engl.* **1996**, *35*, 1154–1196; d) B. Rybtchinski, *ACS Nano* **2011**, *5*, 6791–6818.

[9] a) P. Ball, *Chem. Rev.* **2008**, *108*, 74–108; b) B. M. Rosen, C. J. Wilson, D. A. Wilson, M. Peterca, M. R. Imam, V. Percec, *Chem. Rev.* **2009**, *109*, 6275–6540.

[10] J. Düring, A. Hölzer, U. Kolb, R. Branscheid, F. Gröhn, *Angew. Chem.* **2013**, *125*, 8905–8908; *Angew. Chem. Int. Ed.* **2013**, *52*, 8742–8745.

[11] D. Jiao, J. Geng, X. J. Loh, D. Das, T.-C. Lee, O. A. Scherman, *Angew. Chem.* **2012**, *124*, 9771–9775; *Angew. Chem. Int. Ed.* **2012**, *51*, 9633–9637.

[12] R. Krishna Kumar, X. Yu, A. Patil, M. Li, S. Mann, *Angew. Chem.* **2011**, *123*, 9515–9519; *Angew. Chem. Int. Ed.* **2011**, *50*, 9343–9347.

[13] a) B. P. Binks, R. Murakami, *Nat. Mater.* **2006**, *5*, 865–869; b) Z. H. Nie, A. Petukhova, E. Kumacheva, *Nat. Nanotechnol.* **2010**, *5*, 15–25.

[14] a) D. Patra, F. Ozdemir, O. R. Miranda, B. Samanta, A. Sanyal, V. M. Rotello, *Langmuir* **2009**, *25*, 13852–13854; b) E. Glogowski, R. Tangirala, J. B. He, T. P. Russell, T. Emrick, *Nano Lett.* **2007**, *7*, 389–393.

[15] a) R. Tang, C. S. Kim, D. J. Solfiell, S. Rana, R. Mout, E. M. Velázquez-Delgado, A. Chompoosor, Y. Jeong, B. Yan, Z.-J. Zhu, C. Kim, J. A. Hardy, V. M. Rotello, *ACS Nano* **2013**, *7*, 6667–6673; b) D. Patra, A. Sanyal, V. M. Rotello, *Chem. Asian J.* **2010**, *5*, 2442–2453.

[16] X. C. Yang, B. Samanta, S. S. Agasti, Y. Jeong, Z. J. Zhu, S. Rana, O. R. Miranda, V. M. Rotello, *Angew. Chem.* **2011**, *123*, 497–501; *Angew. Chem. Int. Ed.* **2011**, *50*, 477–481.

[17] a) A. R. Clapp, E. R. Goldman, H. Mattoussi, *Nat. Protoc.* **2006**, *1*, 1258–1266; b) I. L. Medintz, T. Pons, K. Susumu, K. Boeneman, A. M. Dennis, D. Farrell, J. R. Deschamps, J. S. Melinger, G. Bao, H. Mattoussi, *J. Phys. Chem. C* **2009**, *113*, 18552–18561; c) A. M. Dennis, D. C. Sotto, B. C. Mei, I. L. Medintz, H. Mattoussi, G. Bao, *Bioconjugate Chem.* **2010**, *21*, 1160–1170.

[18] a) Y. T. Zhang, Y. K. Yang, W. F. Ma, J. Guo, Y. Lin, C. C. Wang, *ACS Appl. Mater. Interfaces* **2013**, *5*, 2626–2633; b) W. J. Fang, X. L. Chen, N. F. Zheng, *J. Mater. Chem.* **2010**, *20*, 8624–8630.

[19] a) I. L. Medintz, T. Pons, J. B. Delehanty, K. Susumu, F. M. Brunel, P. E. Dawson, H. Mattoussi, *Bioconjugate Chem.* **2008**, *19*, 1785–1795; b) A. M. Dennis, W. J. Rhee, D. Sotto, S. N. Dublin, G. Bao, *ACS Nano* **2012**, *6*, 2917–2924.

[20] G. Sahay, W. Querbes, C. Alabi, A. Eltoukhy, S. Sarkar, C. Zurenko, E. Karagiannis1, K. Love, D. Chen, R. Zoncu, Y. Buganim, A. Schroeder, R. Langer, D. G. Anderson, *Nat. Biotechnol.* **2013**, *31*, 653–658.

[21] a) P. Erbacher, A. C. Roche, M. Monsigny, P. Midoux, *Exp. Cell Res.* **1996**, *225*, 186–194; b) P. S. Ghosh, C.-K. Kim, G. Han, N. S. Forbes, V. M. Rotello, *ACS Nano* **2008**, *2*, 2213–2218; c) S. R. Bhattarai, E. Muthuswamy, A. Wani, M. Brichacek, A. L. Castaneda, S. L. Brock, D. Oupicky, *Pharm. Res.* **2010**, *27*, 2556–2568.

[22] E. A. Mahmoud, J. Sankaranarayanan, J. M. Morachis, G. Kim, A. Almutairi, *Bioconjugate Chem.* **2011**, *22*, 1416–1421.

[23] a) M. P. Gillmeister, M. J. Betenbaugh, P. S. Fishman, *Bioconjugate Chem.* **2011**, *22*, 556–566; b) K. Mellert, M. Lamla, K. Scheffzek, R. Wittig, D. Kaufmann, *PLoS One* **2012**, *7*, e52473.

[24] K. W. Woodburn, N. J. Vardaxis, J. S. Hill, A. H. Kaye, D. R. Phillips, *Photochem. Photobiol.* **1991**, *54*, 725–732.